STRESS PATTERN NEAR THE SAN ANDREAS FAULT, PALMDALE, CALIFORNIA, FROM NEAR-SURFACE IN SITU MEASUREMENTS

Marc L. Sbar

Department of Geosciences, University of Arizona, Tucson, Arizona 85721

Terry Engelder and Richard Plumb[1]

Lamont-Doherty Geological Observatory, Palisades, New York 10964

Stephen Marshak

Department of Geosciences, University of Arizona, Tucson, Arizona 85721

Abstract. We made 29 in situ doorstopper strain relaxation measurements distributed among eight sites spaced on a 35-km transect running from the foothills of the San Gabriel Mountains, across the San Andreas fault, into the western Mojave desert southeast of Palmdale, California. This was a pilot study to test if such measurements can detect the regional stress field and any modification of it in a tectonically complex area. Strain was measured by overcoring strain gauge rosettes which had been bonded to the flattened bottom of a shallow borehole. Measurements of stress were repeatable at each site. We found NNE trending maximum compressive stress (σ_1) at our sites farthest from the fault. This orientation is parallel to the σ_1 inferred from fault plane solutions of major southern California earthquakes and compares favorably with deep hydrofracture stress measurements made near our sites. Nearer the San Andreas fault, the orientation of σ_1 was approximately east-west north of the fault, and northwest-southeast to north-south south of the fault. The repeatability of measurements at a site and the favorable comparison of our measurements with Tullis' [1977] near-surface stress measurements suggest that we reliably determined the stress field orientation present at a site. It was not possible, using the available data, to distinguish the stress caused by residual or topographic effects from tectonically applied stress or to account for modification of the stress field by decoupling across fractures.

Introduction

This paper reports the results of a pilot study designed to test whether in situ strain relaxation measurements can detect the detailed tectonic stress field in a tectonically complex area. Our study concerned the area in the vicinity of a locked fault with a high rupture potential. Theoretical and photoelastic models of strike-slip faults [Rodgers and Chinnery, 1973; Barber and Sowers, 1974] predict that a reorientation of stress trajectories occurs near faults across which there has been strain accumulation. The degree of reorientation is directly related to the strain accumulation. Thus measurement of this stress pattern may provide important information about the dimensions and long-range timing of the eventual rupture on the fault. Since fault plane solutions are in general not available for locked faults, in situ measurements are currently the only way of determining the configuration of the stress field.

Our study focused on a section of the San Andreas fault within the Palmdale uplift, a feature discovered by Castle et al. [1974] during an examination of geodetic leveling data. Two models for the uplift, one relating it to dilatancy of the crust [Wyss, 1977] and one relating it to aseismic creep at depth [Thatcher, 1976], suggest that the uplift may be a manifestation of tectonic strain buildup and may be a precursor of a major earthquake. The last rupture of the San Andreas fault between Chalome and Cajon Pass occurred in 1857. Prescott and Savage [1976] have shown that shear strain is accumulating in a right lateral sense at a rate of 0.2 μ strain/yr over a 10- to 15-km aperture across the fault near Palmdale. Yet data from small-aperture triangulation nets [Meade and Small, 1966; Hofmann, 1968] indicate that creep is not occurring along this section of the fault. In addition, the San Andreas fault within the Palmdale uplift has been almost aseismic for the past forty years [Hileman et al., 1973; Fuis et al., 1977]. An increase in low-level earthquakes ($\geq M_L = 3$), however, has been reported for 1976 and 1977 by McNally and Kanamori [1977]. Such information suggests that strain is accumulating in this region, and if the models apply, there should be a modification of the stress trajectories near the fault.

To test for the effect of the locked San Andreas fault on the regional stress field, we made 29 in situ measurements at eight sites spaced along a broad profile perpendicular to the San Andreas fault, southeast of Palmdale. Stress orientations were measured using a strain relaxation technique that employs a strain cell similar to the one described by Stephenson and Murray [1970] and Leeman [1971]. This strain cell is commonly known as the doorstopper. Our data are compared with those inferred from other in situ stress measurement techniques, fault plane solutions and Neogene geologic structures to evaluate the reliability and applicability of near-surface in situ stress measurements to tectonic problems.

[1]Also at Department of Geological Sciences, Columbia University, New York 10025

Paper number 8B0899.
0148-0227/79/018B-0899$01.00

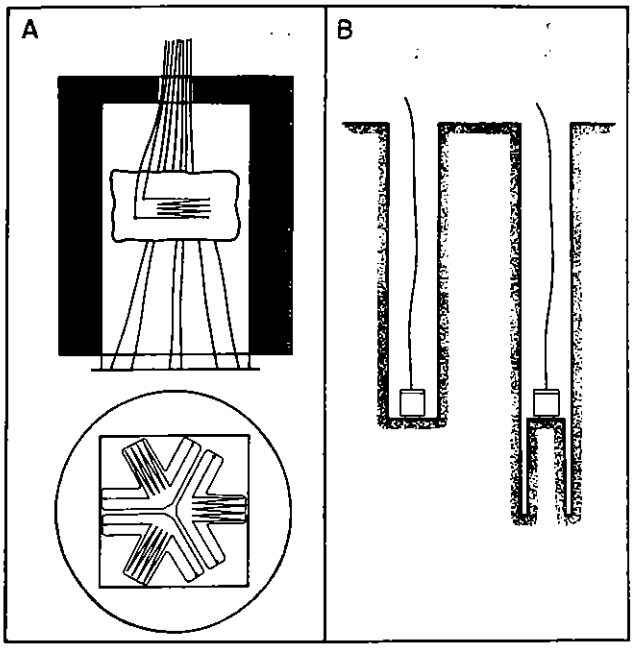

Fig. 1. (a) Cross section and bottom views of a doorstopper. In the cross section, patterned area is hard plastic, nonpatterned area is Dow-Corning RTV and Silguard (low-modulus rubber). Embedded in the Silguard is a thermal compensation gauge consisting of a strain gauge bonded to a wafer of granite. Thick lines are lead wires. Bottom view shows the strain gauge rosette. The doorstopper is about 5 cm high and 2.5 cm in diameter. (b) Cross-sectional view of gauge bonded in drill hole before and after overcoring.

Technique and Data Reduction

Strain relaxation techniques involve measurement of the strain which occurs as a rock is decoupled from the surrounding rock mass. The stress that had been exerted on the rock prior to decoupling may be calculated from the strain relaxation observed if data on the mechanical properties of the rock are also known.

Our doorstopper (Figure 1a) consists of a hard plastic cylinder which contains a low-modulus plastic (Dow-Corning RTV and Silguard). At the base of the RTV is a strain gauge rosette consisting of three foil-resistance strain gauges along radii spaced 120° apart. A thermal compensation gauge, consisting of a strain gauge bonded to a wafer of Barre granite, is embedded in the Silguard above the RTV. The resistance of this gauge is balanced against that of the active components of the rosette using an ac resistance bridge. The thermal compensation gauge is necessary to minimize the thermal effect of drilling water on the strain readings. To reduce this effect further, we let the water flow before overcoring until the readings stabilized.

The strain gauge rosette is exposed at the end of the doorstopper and is epoxied to the flattened bottom of a borehole. When bonded, each gauge covers an area of 21 mm^2 between 1 and 8 mm, as measured from the center of the core along a radius. Figure 1b shows a cross section of the gauge and borehole before and after overcoring. We used an NW oversize diamond drill bit (79-mm O.D.), which produced a 55-mm core, for drilling both the initial hole and the overcore. Two boreholes were drilled at each site with two or three measurements in each hole, made at depths ranging from 0.5 to 3 m. Our technique differs from standard doorstopper methods in that we run a cable from the doorstopper through the drill string to our strain indicator to allow readings during overcoring. Thus, we were able to recover data even if the core broke before the drilling was completed. We calculated the maximum and minimum principal strains (ε_1 and ε_2 respectively) and their orientation from the strain observed on the three gauges of the rosette.

To transform strain to stress, it is necessary to have data on the mechanical properties of samples. The mechanical property we measured in the field is similar to linear compressibility, as defined by Nye [1957, p. 146]: The linear compressibility of a crystal is the relative decrease in length of a line when the crystal is subjected to unit hydrostatic pressure. This definition applies to a uniform three-dimensional load. In our experiment, as described below, the sample is stressed radially but is not constrained axially. Because this is a two- rather than a three-dimensional test, for the purpose of this report, we define the resulting value, which relates stress to strain, as the pseudo-linear compressibility (PLC).

The PLC is related to the strain (ε_i) measured during radial compression and to the known pressure (P) applied by the cylindrical test chamber, by the formula

$$PLC = \frac{\varepsilon_i}{P} = \frac{1-\nu_i}{E_i} \qquad (1)$$

where ν_i is Poisson's ratio and E_i is Young's modulus for stress applied parallel to ε_i [Jaeger and Cook, 1969, p. 134]. In the above, two-dimensional orthorhombic symmetry is assumed.

All of our cores are anisotropic to some degree, as shown by the variation of PLC with direction (Table 1). Using the value of PLC parallel to each of the three gauges of the strain rosette, we can transform the strain measured on each gauge during overcoring to the stress which was exerted parallel to that gauge prior to overcoring by the formula

$$\sigma_{oc} = \varepsilon_{oc}/PLC \qquad (2)$$

where ε_{oc} is the strain that occurred during overcoring and σ_{oc} is the corresponding stress. Effectively, this is a transformation from tensor strain to tensor stress which, to a first approximation, incorporates the anisotropy of the sample. From the three components of stress, the principal stresses and their orientations may be easily calculated.

The measurements of PLC were done in the field using a cylindrical test chamber on cores with doorstoppers still attached (Figure 2). A uniform radial stress was applied to the core

TABLE 1. Strain, Material Properties, and Calculated Stress for All Overcores

			Strain				Pseudolinear Compressibility					Stress			
Site	Hole	Depth, cm	ε_1, $\times10^{-6}$	ε_2, $\times10^{-6}$	Azimuth of ε_1	Ratio	Applied Pressure, bars	Max, bars^{-1} $\times10^{-6}$	Min, bars^{-1} $\times10^{-6}$	Azimuth of Max	Percent Anisotropy	σ_1, bars	σ_2, bars	Azimuth of σ_1	Ratio
1	A	71	708	409	N67°W	1.7									
		201	1098	413	N59°W	2.7	17	54.6	18.8	N52°E	65	37.9	2.7	N54°W	14
		279	1060	484	N48°W	2.2	13.6	26.6	18.2	N15°E	31	44.4	13.2	N56°W	3.4
	B	79	862	706	N78°W	1.2									
		137	966	316	N64°W	3.1	13.6	72.7	31.5	N23°E	57	24.2	0.4	N62°W	60.5
			(930)	(475)	(N60°W)	(2.0)		(49.4)	(24.8)	(N34°E)	(50)	(35.4)	(5.5)	(N57°W)	(6.4)
2	A	91	534	353	N16°W	1.5	14.3	41.9	21.0	N78°W	50	19.0	5.7	N-S	3.3
		147	762	345	N8°W	2.2	17	33.5	25.8	N13°W	23	18.6	11.4	N8°W	1.6
	B	107	391	313	N46°W	1.2	15.3	28.0	17.8	N18°W	36	16.1	9.5	N9°W	1.7
			(544)	(355)	(N7°W)	(1.5)		(32.2)	(23.8)	(N76°W)	(26)	(17.8)	(9.1)	(N-S)	(2.0)
3	A	58	72	-33	N22°E		13.6	14.7	12.4	N58°E	16	4.0	-2.9	N24°E	
		89	65	-49	N25°E		13.6	23.9	16.8	N35°W	30	3.3	-0.1	N44°E	
	B	79	71	-2	N39°E		13.6	17.0	12.4	N7°W	27	0.6	-1.5	N32°E	
		104	9	-28	N33°E			(17.6)	(14.8)	(N21°W)	(16)	(2.5)	(-1.4)	(N31°E)	
			(71)	(-32)	(N23°E)										
							13.6	22.4	13.2	N1°W	41	15.7	-31.7	N88°E	
4	A	46	394	-890	N89°E										
		64	124	73	N86°W										
	B	150	544	76	N63°W										
			(327)	(-220)	(N84°W)			(22.4)	(13.2)	(N1°W)	(41)	(15.7)	(-31.7)	(N88°E)	
5	A	120	300	168	N81°E	1.8									
	B	71	454	77	N84°E	5.9	13.6	30.6	24.2	N76°E	21	12.5	2.7	N87°E	4.6
		152	1356	15	N69°E	90.6									
		188	142	-67	N81°E										
			(556)	(55)	(N74°E)	(10.1)		(30.6)	(24.2)	(N76°E)	(21)	(12.5)	(2.7)	(N87°E)	(4.6)
6	A	147	100	2	N63°E	50	13.6	12.4	6.3	N32°E	49	7.6	1.2	N70°E	6.3
		213	134	37	N80°W	3.6	13.6	17.4	12.4	N14°E	29	8.6	1.8	N76°W	4.8
	B	152	60	-45	N55°E		13.6	7.8	6.2	N49°E	23	6.3	-4.8	N54°E	
		203	86	7	N81°E	12.3	13.6	13.2	6.7	N30°E	49	8.0	0.8	N84°W	10.0
			(86)	(9)	(N73°E)	(9.6)		(12.6)	(8.0)	(N28°E)	(37)	(6.6)	(0.7)	(N78°E)	(9.4)
7	A	152	157	-20	N2°E										
		226	253	42	N1°E	6.0	13.6	24.1	10.2	N8°E	57	8.9	4.7	N7°W	1.9
	B	183	124	-63	N40°E		13.6	10.1	9.3	N22°E	9	1.0	-5.2	N40°E	
			(160)	(4.2)	(N13°E)	(38.1)		(17.1)	(9.8)	(N9°E)	(43)	(8.7)	(0.7)	(N32°E)	(12.4)
8	A	71	132	35	N15°E	3.8	13.6	4.5	2.4	N30°W	47	32.9	8.2	N34°E	4.0
	B	107	111	-17	N24°E										
		170	75	33	N7°E	2.3									
			(105)	(18)	(N18°E)	(5.8)		(4.5)	2.4)	(N30°W)	(47)	(32.9)	(8.2)	(N34°E)	(4.0)

ε_1 and ε_2 and σ_1 and σ_2 are principal strains and stresses, respectively. Ratio is max/min. Anisotropy is (max - min)/max. The applied pressure is the radial stress at which the pseudolinear compressibility was measured. Averages are given in parentheses; all of the averages are tensor averages.

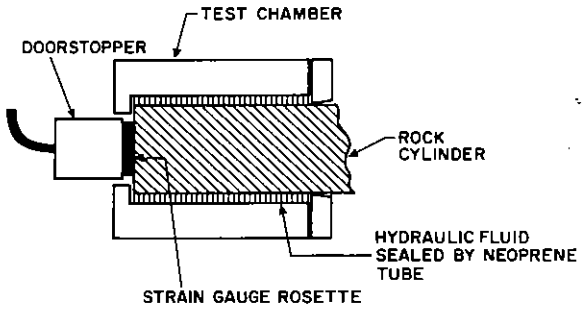

Fig. 2. Cross section of a test chamber designed to apply a radial stress on an NW size core (55-mm diameter).

incrementally from zero to about 40 bars and was then returned incrementally to zero. This was done twice for each sample. We observed a nonlinear relation between load and strain and only a partial recovery of the strain upon removing the stress. This behavior is commonly observed in rocks subjected to low stresses and is due to the closing of existing microcracks and the formation of new microcracks. Due to the inelastic behavior of the samples, there may be errors in choosing the proper magnitude of PLC for the stress calculation. The orientation of maximum PLC remains the same for all loading cycles, however, so calculated stress orientations did not incorporate errors due to inelasticity. The first increment of pressure applied during testing was usually 13.6 bars, because this was the lower limit of resolution of our pressure gauge. This value produced strains similar to those observed during overcoring, so we arbitrarily used the PLC measured at 13.6 bars for most of our calculations of stress.

Equation (1) is exact for a radial load, but the stresses exerted on the rock in the field are not equal in all directions. Thus, there is an error inherent in the transformation from stress to strain. Fortunately, this error does not significantly change the calculated orientation of the principal stresses, although it does affect their magnitude.

A further correction must be applied to the stress data to account for the concentration of stress that occurs at the end of a borehole. We used an experimentally derived correction suggested by Leeman [1971]:

$$\sigma_1 = \sigma_1' + 0.75(0.645 + \nu)\sigma_2 \qquad (3)$$

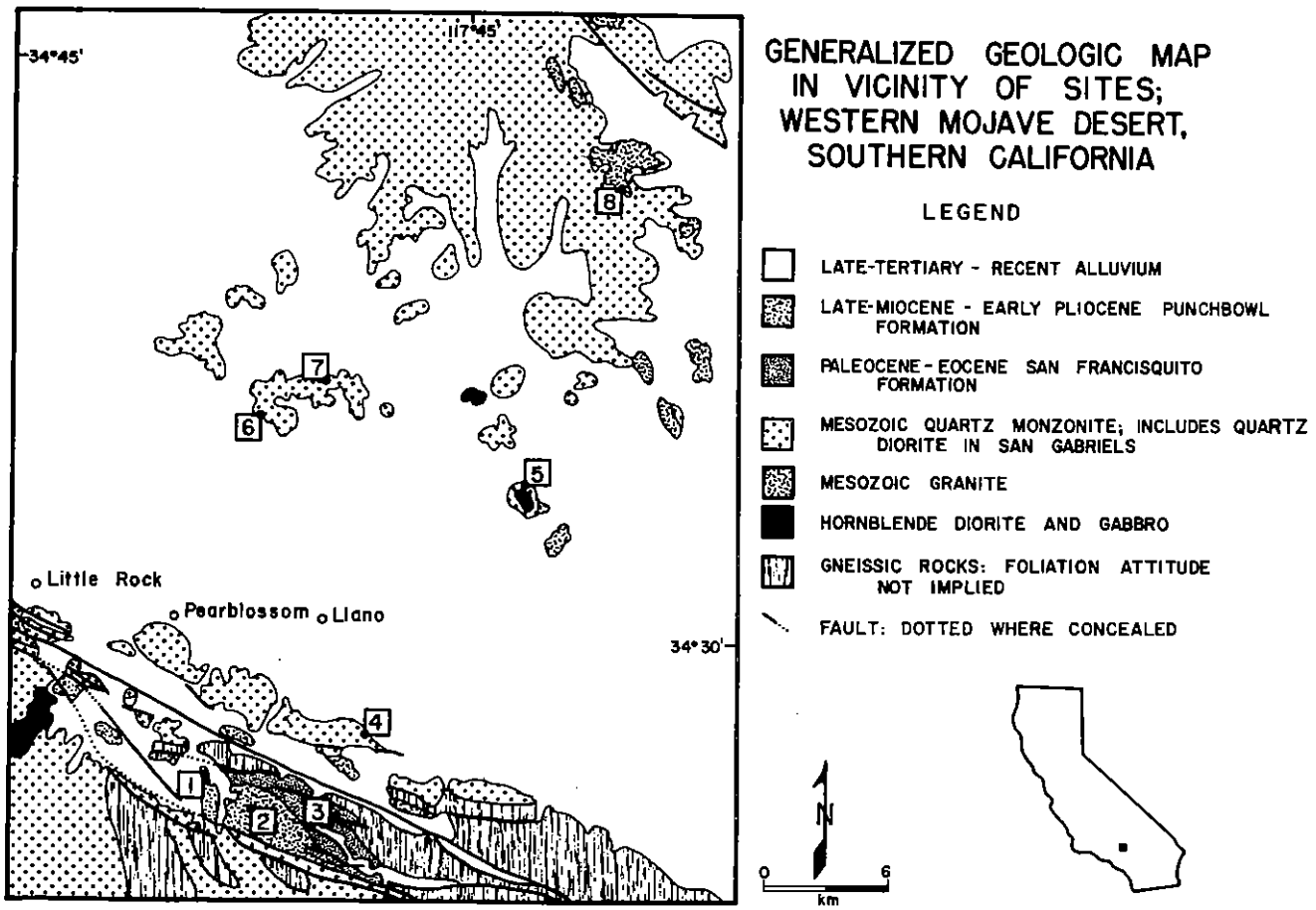

Fig. 3. Map of generalized geology in the vicinity of in situ stress measurement sites, western Mojave Desert, and foothills of the San Gabriel Mountains. The sites are numbered. The longest continuous fault in the southern part of the map is the San Andreas. The Punchbowl fault and various subsidiary faults are also shown. Location is shown in inset and as box in Figure 6. Geology simplified from Dibblee [1967].

where σ_i is one component of the applied stress in the earth, σ_i' is the stress computed from strain relaxation at the end of a borehole, ν is Poisson's ratio (which we take as 0.25), and σ_z is the vertical stresses assumed to equal density times gravitational acceleration times depth. This correction does not change the direction of the principal stresses. Once we applied all of the corrections, we calculated tensor averages for all the reliable stress and strain measurements at a given site (Table 1).

Site Description

We obtained measurements at eight sites spaced along a 35-km northeast-trending transect which ran from the foothills of the San Gabriel Mountains near Valyermo to Adobe Mountain in the western Mojave desert. Our sites were located in intrusive, metamorphic, and sedimentary rocks (Figure 3). Finding suitable outcrop was often challenging.

Sites 1 and 2 were drilled in the low-lying ridges of the upper Miocene Punchbowl formation between the San Andreas and Punchbowl faults. Here the Punchbowl formation consists of massive, light buff, cross-bedded, coarse terrestrial sandstone with large lenses of pebble and cobble conglomerate [Noble, 1954]. The formation is remarkably unfractured, although there are bedding plane fractures spaced at 1- to 3-m intervals and some vertical joints with locally varying attitudes, spaced at 3- to 7-m intervals. Our sites were on the north limb of a large syncline whose axis strikes N70°W and plunges west. At our sites the attitude of the beds is N50-60°W, 45°SW. We made an effort to avoid the conglomerate and set our gauges on the homogeneous sandstone. Site 1 was a flat outcrop surrounded by alluvium, while site 2 was on the floor of a wash bounded by 9-m-high 25° rock slopes.

Site 3 was located in the base of the San Gabriel foothills along Little Rock Creek in a unit of Paleocene marine clastics called the San Francisquito formation [Dibblee, 1967]. The formation consists of interbedded conglomerates, shales, and sandstone. Our site was in a medium-grained buff sandstone layer about 4 m thick, bounded by shale layers and oriented N20-25°W, 35°SW. The fracture spacing ranges from 0.3-1 m in this sandstone. Steeply dipping joints on the outcrop strike N5-10°E, N62-75°W, and N40°E.

Site 4 was located at the base of a roadcut in Bob's Gap, a pass through a ridge parallel to and just northeast of the San Andreas fault. Noble [1954] names the rock at this location Holcombe quartz monzonite and suggests that it is of Mesozoic age. Where we drilled, the rock is foliated and has a cataclastic fabric.

Sites 5-8 were drilled in the Mesozoic intrusive rocks which form the basement of much of the western Mojave. Gravity data [Mabey, 1960] indicate that in the western Mojave, there are two northeast trending basement highs separating three alluvium-filled basins. Our sites were along the bases of buttes associated with the southern basement high. Site 5 was in a medium-grained quartz monzonite that rings the base of Black Butte, so called because of a core of hornblende diorite. Site 6 was drilled on the west side of Lovejoy Buttes in a fresh coarse-grained quartz monzonite. Site 7 was beside a man-made pond in a saddle of Lovejoy Buttes. The rock at site 7 is similar to that of site 5. Site 8 was drilled in the wide pediment surrounding Adobe Mountain. The rock here is a fine-grained granite, cut by pegmatite dikes. At all of these sites, steeply dipping joints were spaced from 10 cm to 1 m. Horizonatal joints were observed as well. The local relief is about 10 m at sites 6 and 7, negligible at site 8, and significant at site 5, which was only 30 m from the 20° slopes of Black Butte.

The steeply dipping joints at site 5 strike N80°W, N40°W, and N60°E; at site 6 they are east-west to N70°W, N30-40°W, and N7°W; at site 7 they strike N85°E and N30-40°E; and at site 8 they are N20°E, N80°E to east-west, N40°W, and north-south.

Data

We made 29 successful strain relaxation measurements over the course of 1 month in the field. Usually, six measurements were attempted at each of the eight sites, but failures occurred because of fractures beneath or near the gauges and because of separation of the wires in the gauge. Because we did not always obtain the 10-cm-length core necessary for mechanical tests, only 18 stress calculations could be made. All our data--strain relaxation, PLC, and stress--are tabulated in Table 1.

Strain relaxation was measured incrementally during overcoring. Strain increased until the overcoring depth was about 1/2 the core diameter. It then decreased until drilling reached a depth of one core diameter, at which point it leveled off. Hoskins [1967] and Stephenson and Murray [1970] report similar strain versus overcoring depth behavior.

The variation in orientation of the principal strains at the individual sites range from 15° to 45° for measurements where the ratio of maximum to minimum strain is greater than 1.5. At a site, the magnitudes of the principal strains were similar, but between sites, the variation in magnitude was more than a factor of 10.

For cores with mechanical anisotropies greater than 15%, the range in orientation of the maximum PLC at the individual sites is 35° to 79°. This is slightly greater than the variation in orientation for the principal strains. The sites with the greatest anisotropy had the least scatter, and vice versa. In general, the ratio of maximum to minimum PLC was lower than the ratio of maximum to minimum strain. The anisotropy of the cores varied from 9% to 65%.

At sites 7 and 8, farthest from the San Andreas fault, σ_1 (tensor average) trends NNE. At sites 4, 5, and 6 the next closest on the northeast side, σ_1 trends ENE to east-west. Sites 1, 2, and 3 southwest of the fault show a σ_1 varying from N60°W parallel to the fault to N30°E. All three sites were equidistant from the trace of the 1857 fault break on the San Andreas.

Data Interpretation

The strain relaxation observed at a site is influenced not only by regional tectonic stress,

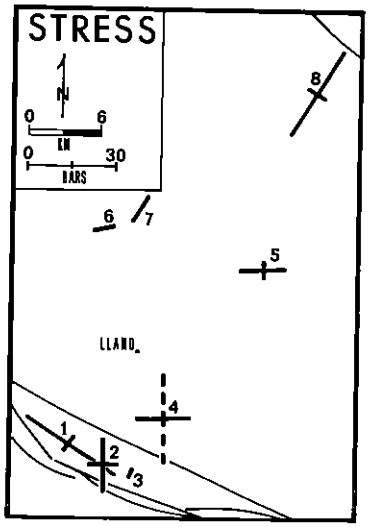

Fig. 4. Tensor averages of the maximum and minimum horizontal stress at each site in the vicinity of the Palmdale uplift, southern California. Dashed lines indicate tensional stress. The map is approximately the same as Figure 3.

but also by topographic stress, residual stress, and the degree of outcrop coupling across fractures. One of the difficulties of near-surface strain relaxation measurements is the estimation of the relative contributions of regional tectonic stress and of noise sources for each measurement.

Residual stress is locked into a rock during the course of its thermal, tectonic, and burial history. Its presence can be determined by double overcoring. In this procedure, a second overcore is drilled within the first. The strain measured during the second overcore represents residual stress because the core has already been uncoupled from all applied stress. Time constraints allowed us to make double overcores only in the sedimentary rocks of site 1. No significant residual stress was observed at that site.

Both topographic and regional tectonic stress are external applied stresses. Topography may add a component of stress to the regional tectonic stress in two ways. First, lithostatic loading at the base of hill slopes can cause a Poisson expansion perpendicular to the mountain front or to the axis of a valley [Jaeger and Cook, 1969, pp. 356-358]. Second, the slope of valleys causes a concentration to tectonic stress perpendicular to the valley axis [Harrison, 1976]. Sites 3, 4, and 5 were adjacent to steep-sided slopes; of these, sites 3 and 4 were in valleys. Only at site 4 was σ_1 perpendicular to a valley axis. Topographic stress may be superimposed on the tectonic stress at sites 3 and 5, although σ_1 was not perpendicular to the slopes in either case. From our measurements it is difficult to quantify the effect topography had on the in situ stress measured at sites 3, 4, and 5.

Coupling of the outcrop on which the measurements are made to the earth is a problem which appears to affect the magnitude and possibly the direction of the stress observed. Engelder and Sbar [1977] found that the magnitude and reproducibility of surface strain relaxation measurements in northern New York appeared to be directly proportional to the horizontal dimensions of blocks bounded by vertical joints. If coupling across horizontal joints were a significant problem, we would expect a noticeable difference in measurements above and below sheet fractures. We did not observe this difference.

The mechanical properties of strata below the outcrop where a measurement is made may also weaken the coupling to earth strain at depth. For example, the formation at site 3 is a sequence of interbedded sandstones and shales. Since we observed very low stress there (Figure 4 and Table 1), we suspect that coupling may have been poor across the shaly layers.

We cannot easily explain the large negative stress observed at site 4. It should be noted, however, that this value is due to the unusually large contraction recovered in only one of the three measurements made at that site. If that measurement were discounted, the stress would not be negative. The trend of all three measurements is similar, so the direction of the tensor average is not seriously affected by this one measurement.

The variation in magnitude of the principal stresses from site to site, as shown in Figure 4, may not represent a real variation in the stress at depth but may be a function primarily of the coupling of the outcrop to the earth. The largest magnitude for the maximum compressive stress (σ_1) that we measured is about 35 bars. This may represent a lower limit for the near-surface stress in the survey area. Because of our skepticism about the magnitude of stress determined, we normalized the data in Figure 5, maintaining the ratio of σ_1 to least compressive stress (σ_2). It is also possible that coupling may be anisotropic, affecting the orientation, as well as the magnitude, of stress.

Tullis [1977] made strain relaxation measurements, using the U. S. Bureau of Mines borehole deformation gauge, at four sites near ours. His results are quite similar to ours both in orientation of principal stresses and in the variation of magnitude from site to site. Because of the favorable comparison of our measurements with others obtained near the surface in the same area, we feel that our results are not merely an artifact of our measurement technique but are representative of the stress field in existence at the sites.

Discussion: The Relation Between In Situ Stress and Southern California Tectonics

Regional tectonic stress is caused by large-scale forces related to plate interactions. Such stress is ultimately responsible for the tectonic fabric of an area. Thus, one can gain a feeling for the gross aspects of the tectonic stress in an area by looking at recent tectonic activity in that area.

Southern California is divided into many structurally discrete tectonic blocks, each of which appears to have responded differently to stresses applied through time [Jahns, 1973]. The block

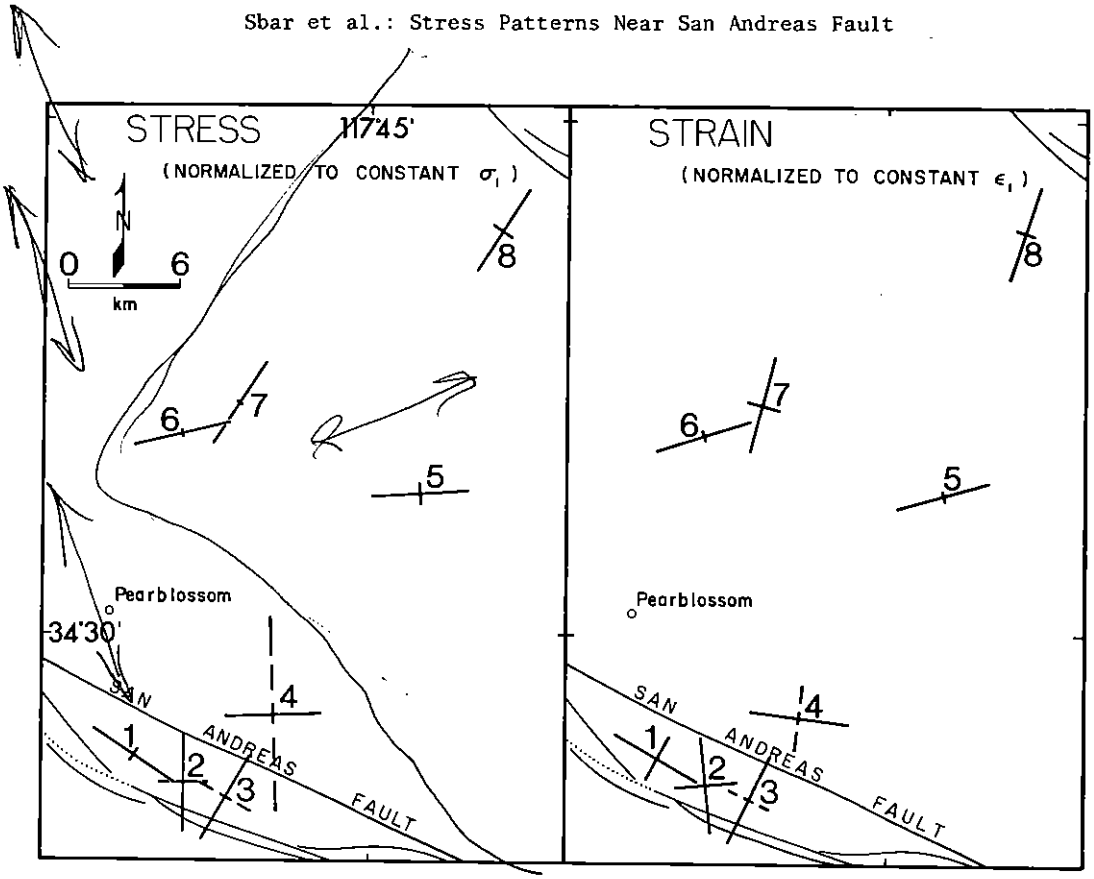

Fig. 5. Maps of stress and strain in the vicinity of the Palmdale uplift, southern California: Strain orientations were measured directly. Maximum elongations shown are normalized. Minimum elongations are adjusted so that the correct ratio of max to min is maintained. Minimum strains are dashed when negative (rock contraction). The stress representations are calculated from the strains by adjusting for linear compressibility. Maximum compressive stress are also normalized. Minimum compressive stresses were adjusted accordingly to maintain the correct ratio. They are dashed when negative (i.e., for site 4, maximum compressive stress is approximately E-W, not N-S). The map is approximately the same as Figure 3.

boundaries outline in Figure 6 originated in Miocene time, subsequent to the subduction of the Farallon spreading ridge and the initiation of transform faulting that has continued to the present [Atwater, 1970]. Our measurements were made in the western Mojave block and adjacent to the San Andreas fault along the eastern margin of the Western Transverse Ranges block.

The Mojave block is bounded on the north by the Garlock fault, on the southwest by the San Andreas fault, and on the south by the Eastern Transverse Ranges. The eastern boundary which separates the Mojave block from the Basin and Range province is not physiographically defined. The Mojave block may be subdivided into two subunits defined by their degree of tectonic activity [Bull, 1977]. Based on geomorphic evidence, Bull suggests that the eastern subunit has been tectonically active in Holocene time. Seismic evidence indicates that this activity is continuing into the present [Hileman et al., 1973; Fuis et al., 1977]. The major tectonic features are northwest oriented strike-slip faults on which there has been a significant dip-slip component of movement. The western Mojave subunit is basically tectonically inactive--there are few earthquakes and no geomorphic evidence of Holocene movement.

The San Andreas fault in central California has a straight trace striking approximately N40°W. Where it borders the Mojave block, it assumes a strike of N70°W. The vector of relative plate motion between the North American plate and the Pacific plate strikes about N40°W [Minster et al., 1974] and is not parallel to the trace of the San Andreas in the area of the bend. Compressive stresses have developed in this region as the Pacific plate abuts the North American plate, uplifting the Transverse Ranges which are characterized by east-west striking folds and faults. The thrusting mechanisms of the Kern County and San Fernando earthquakes are recent evidence of such deformation. Even though both thrusting and strike-slip fault plane solutions are found throughout southern California, the range in azimuth of the P axes of these mechanisms is only 40° (Figure 6). One can infer from this that the regional trend of σ_1 is north to NNE with a nearly horizontal dip. This orientation is consistent with Neogene geologic deformation [Allen et al., 1965; Jahns, 1973; Bull, 1977].

The goal of this research is to determine if we can measure the regional tectonic stress and its modification in the vicinity of a fault with a high earthquake potential. Such modification can be caused by buildup of strain across the fault, by the geometry of the fault, and by local strain release in the form of earthquakes. Parameters such as residual stress and topo-

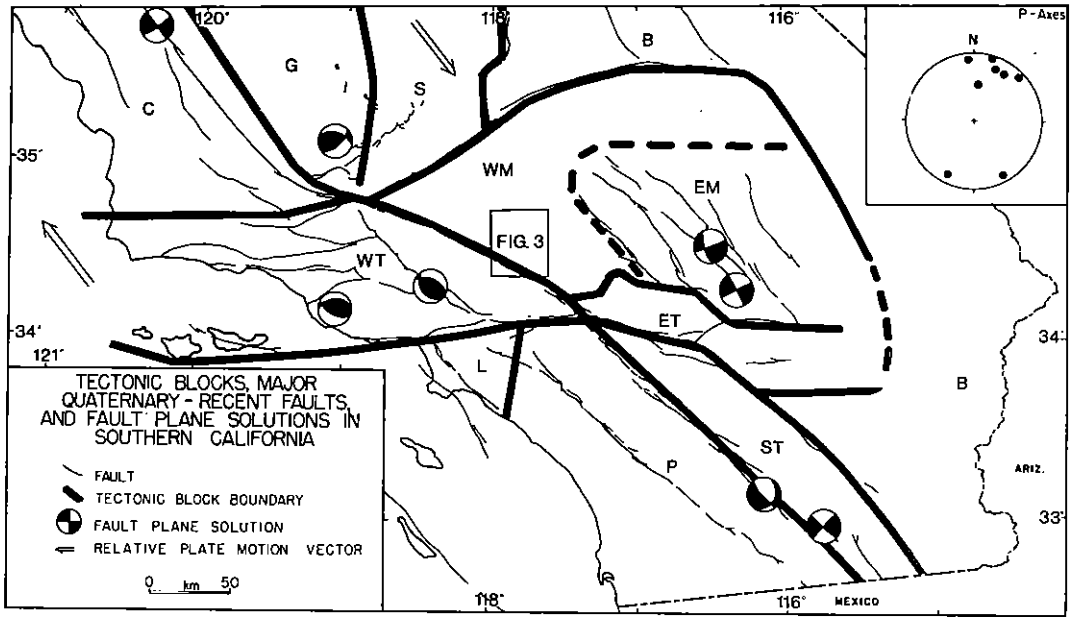

Fig. 6. Map of southern California showing the approximate boundaries of tectonic blocks (regions characterized by a distinctive structural style). C = Coast Ranges, G = Great Valley, S = Sierra Nevada, B = Basin and Range, WM = Western Mojave (tectonically inactive), ET = Eastern Transverse Ranges, WT = Western Transverse Ranges, ST = Salton Trough, P = Peninsular Ranges, L = Los Angeles Basin. Also shown are the relative plate motion vectors (length not significant) and fault plane solutions of characteristic earthquakes. A lower hemisphere equal-area projection of P axes for those solutions is shown in the upper right hand corner. The faults shown are major Quaternary-Historic faults [Bull, 1977; Minister et al., 1974; Gutenberg, 1955; Allen and Nordquist, 1972; McEvilly et al., 1967; Dillinger, 1973; Kanamori and Fuis, 1976; Thatcher and Hamilton, 1973; Stillman and Ellsworth, 1976].

graphic stress are, in essence, noise which may obscure the tectonic stress.

At sites 7 and 8, most distant from the fault, our calculated σ_1 is oriented NNE, approximately parallel to the maximum regional tectonic stress inferred from fault plane solutions and Holocene structures. At sites 4, 5, and 6, just north of the fault, σ_1 was oriented close to E-W. At sites 1 and 2, just south of the fault, σ_1 was oriented close to NW. The extremely low magnitude of strain measured and the poor outcrop conditions at site 3 require us to discount this measurement. These observations are consistent with the modification of the tectonic stress field by the San Andreas fault. We cannot demonstrate this conclusively, since at this time, we are unable to separate the applied tectonic stress from noise caused by residual and topographic stresses or from variations in outcrop coupling.

Temporal variations in the stress field may also be significant. McNally et al. [1978] demonstrated that σ_1 varied as much as 90° in azimuth over a 10-month period. Their results come from fault plane solutions of small earthquakes in the Juniper Hills area several kilometers northwest of site 1.

Conclusions

In situ doorstopper strain relaxation measurements south of Palmdale are repeatable at a site and compare favorably with other measurements made near the surface and at depth in the same area. They are consistent with a model in which the regional tectonic stress field is modified by the San Andreas fault zone, but we cannot eliminate other possible sources for the stress observed. Residual and topographic stress, as well as decoupling across fractures and bedding planes, may influence our measurements. A high density of stress measurements, which could be statistically treated, may surmount this problem.

Acknowledgments. We acknowledge the assistance of Tony Lomando in fabricating the doorstoppers used in this experiment. Terry Tullis helped us in the field logistics. Christopher Scholz and Roger Bilham critically reviewed this manuscript. This research was supported by the U. S. Geological Survey under grant number 14-08-0001-0417 to the University of Arizona and 14-08-0001-0404 to Lamont-Doherty Geological Observatory. Lamont-Doherty Geological Observatory contribution 2750.

References

Allen, C. R. and J. M. Nordquist, Foreshock, main shock and larger aftershocks of the Borrego Mountain earthquake, U. S. Geol. Surv. Prof. Pap. 787, 16-23, 1972.

Allen, C. R., P. St. Amand, C. F. Richter, and J. M. Nordquist, Relationship between seismicity and geologic structure in the southern California region, Bull. Seismol. Soc. Amer., 55, 753-797, 1965.

Atwater, T. M., Implications of plate tectonics for the Cenozoic tectonic evolution of western

North America, Geol. Soc. Amer. Bull., 81, 3513-3536, 1970.
Barber, D. W. and G. M. Sowers, A photoelastic study of the effects of surface geometry on fault movements, in Advances in Rock Mechanics, pp. 585-590, International Society for Rock Mechanics, Denver, CO, 1974.
Bull, W. B., Tectonic geomorphology of the Mojave Desert, semi-annual grant report, 200 pp., Office of Earthquake Stud., U. S. Geol. Surv., Menlo Park, CA, 1977.
Castle, R. O., J. N. Alt, J. C. Savage, and E. I. Balazs, Elevation changes preceding the San Fernando earthquake of February 9, 1971, Geology, 2, 61-66, 1974.
Dibblee, T. W., Jr., Areal geology of the western Mojave Desert, California, 153 pp., U. S. Geol. Surv. Prof. Pap. 522, 1967.
Dillinger, W. H., Focal mechanism of San Fernando earthquake, in San Fernando, California, earthquake of February 9, 1971, vol. III, edited by L. M. Murphy, pp. 49-68, U. S. Department of Commerce, Washington, DC, 1973.
Engelder, T. and M. L. Sbar, The relationship between in situ strain relaxation and outcrop fractures in the Potsdam sandstone, Alexandria Bay, New York, Pure Appl. Geophys., 115, 41-55, 1977.
Fuis, G. S., M. E. Friedman, and J. A. Hileman, Preliminary catalog of earthquakes in southern California, July 1974-September 1976, Open File Rep. 77-181, 107 pp., U. S. Geol. Surv. Reston, VA, 1977.
Gutenberg, B., The first motion in longitudinal and transverse waves of the main shock and the direction of slip, Earthquakes in Kern County, California During 1952, Calif. Div. Mines Geol. Bull., 171, 165-170, 1955.
Harrison, J. C., Cavity and topographic effects in tilt and strain measurements, J. Geophys. Res., 81, 319-328, 1976
Hileman, J. A., C. R. Allen, and J. M. Nordquist, Seismicity of the southern California region, 1 January 1932 to 31 December 1972, report, 83 pp., Seismol. Lab., Calif. Inst. of Technol. Pasadena, Calif., 1973.
Hofmann, R. B., Geodimeter fault movement investigations in California, Calif. Dep. Water Resour. Bull., 116(6), 183 pp., 1968.
Hoskins, E. R., An investigation of strain rosette method of measuring rock stresses, Int. J. Rock Mech. Mining Sci., 4, 155-164, 1967.
Jaeger, J. C. and N. G. W. Cook, Fundamentals of Rock Mechanics, 515 pp., Chapman and Hill, London, 1969.
Jahns, R. H., Tectonic evolution of the Transverse Ranges Province as related to the San Andreas Fault System, Proceedings of Conference on Geologic Problems of San Andreas Fault System, Stanford Univ. Publ. Geol. Sci., 13, 149-170, 1973.
Kanamori, H. and G. Fuis, Variation of P-wave velocity before and after the Galway Lake earthquake (M_L = 5.2) and the Goat Mountain earthquakes (M_L = 4.7, 4.7), 1975, in the Mojave Desert, California, Bull. Seismol. Soc. Amer., 66(6), 2017-2037, 1976.
Leeman, E. R., The C.S.I.R. Doorstopper and triaxial rock stress measuring instruments, Rock Mech., 3, 25-50, 1971.
Mabey, D. R., Gravity survey of the western Mojave Desert, California, U. S. Geol. Surv. Prof. Pap. 316-D, 73 pp., 1960.
McEvilly, T. V., W. H. Bakum, and K. B. Casaday, The Parkfield, California earthquakes of 1966, Bull. Seismol. Soc. Amer., 57, 1221-1244, 1967.
McNally, K., H. Kanamori, and J. C. Pechmann, Earthquake swarm along the San Andreas fault near Palmdale, southern California, 1976 to 1977, Science, 201, 814-817, 1978.
Meade, B. K. and J. B. Small, Current and recent movement on the San Andreas fault, Calif. Div. Mines Geol. Bull., 190, 385, 1966.
Minster, J. B., T. H. Jordan, P. Molnar, and E. Haines, Numerical modeling of instantaneous plate tectonics, Geophys. J. Roy. Astron. Soc., 36, 541-576, 1974.
Noble, L. F., The San Andreas fault zone from Soledad Pass to Cajon Pass, California, Calif. Div. Mines Geol. Bull., 170, 37-38, 1954.
Prescott, W. H. and J. C. Savage, Strain accumulation on the San Andreas fault near Palmdale, California, J. Geophys. Res., 81, 4901-4908, 1976.
Rodgers, D. A. and M. A. Chinnery, Stress accumulation in the Transverse Ranges, southern California, Proceedings of Conference on the Tectonic Problems of the San Andreas Fault System, Stanford Univ. Publ. Geol. Sci., 13, 70-79, 1973.
Stephenson, B. R. and K. J. Murray, Application of the strain rosette relief method to measure principal stress throughout a mine, Int. J. Rock Mech. Mining Sci., 7, 1-22, 1970.
Stillman, D. J. and W. L. Ellsworth, Aftershocks of the February 21, 1973 Pt. Mugu, California Earthquake, Bull. Seismol. Soc. Amer., 66, 1931-1952, 1976.
Thatcher, W., Episodic strain accumulation in southern California, Science, 194, 691-695, 1976.
Thatcher, W. and R. M. Hamilton, Aftershocks and source characteristics of the 1969 Coyote Mountain earthquake, San Jacinto Fault zone, California, Bull. Seismol. Soc. Amer., 63, 647-661, 1973.
Tullis, T. E., Stress measurements by shallow overcoring on the Palmdale uplift (abstract), EOS Trans. AGU, 58, 1122, 1977.
Wyss, M., Interpretation of the southern California uplift in terms of the dilatancy hypothesis, Nature, 266, 805-808, 1977.

(Received January 9, 1978;
revised July 12, 1978;
accepted August 27, 1978.)